Medical Image Analysis xxx (2012) xxx–xxx

Contents lists available at SciVerse ScienceDirect

Medical Image Analysis

journal homepage: www.elsevier.com/locate/media

Statistical model based shape prediction from a combination of direct observations and various surrogates: Application to orthopaedic research

Rémi Blanc [a,*], Christof Seiler [b], Gabor Székely [a], Lutz-Peter Nolte [b], Mauricio Reyes [b]

[a] Computer Vision Laboratory, ETHZ Zürich, Switzerland
[b] Institute for Surgical Technology and Biomechanics, University of Bern, Switzerland

ARTICLE INFO

Article history:
Received 22 November 2011
Received in revised form 18 April 2012
Accepted 19 April 2012
Available online xxxx

Keywords:
Shape prediction
Linear regression
Computer-assisted orthopaedic research

ABSTRACT

In computer-assisted orthopaedic surgery, recovering three-dimensional patient-specific anatomy from incomplete information has been focus of interest due to several factors such as less invasive surgical procedures, reduced radiation doses, and rapid intra-operative updates of the anatomy. The aim of this paper is to report results obtained combining statistical shape modeling and multivariate regression techniques for predicting bone shape from clinically and surgically relevant predictors, including sparse observations of the bone surface but also morphometric and anthropometric information. Different state of the art methods such as partial least square regression, principal component regression, canonical correlation analysis, and non-parametric kernel-based regression are compared. Clinically relevant surrogate variables and combinations are investigated on a database of 142 femur and 154 tibia shapes obtained from CT images. The results are evaluated using cross validation to quantify the prediction error. The proposed approach enables to characterize the added value of different predictors in a quantitative and localized fashion. Results indicate that complementary sources of information can be efficiently exploited to improve the accuracy of shape prediction.

1. Introduction

In computer-assisted orthopaedic surgery, there is increasing interest in developing technologies to assess bone anatomy pre-, and intra-operatively in a non-invasive way. Furthermore, radiation dose reduction has been acknowledged as an important goal in healthcare, fostering the use of less irradiative technologies (Raisz and Jul, 2005; Task Group on Control of Radiation Dose in Computed Tomography, 2000; Brenner et al., 2007). Additionally, some orthopaedic surgeries such as total hip arthoplasty (THA) and total knee arthoplasty (TKA) usually do not rely on a pre-, or intra-operative computed tomography (CT) scan. Therefore, patient-specific three-dimensional shape reconstruction from sparse information, e.g. acquired from ultrasound (US) or X-ray imaging, clearly appear as highly desirable technologies both for pre-operative planning or for intra-operative navigation. In the last years, methods to reconstruct patient specific bone shape using statistical shape modeling techniques have grown in popularity. For a comprehensive review of statistical shape model applied to medical images the reader is referred to (Heimann and Meinzer, 2009). General approaches as well as modality-specific methods have been developed (Fleute et al., 1999, 2002; Benameur et al., 2003; Chan et al., 2003; Lamecker et al., 2006; Rajamani et al., 2007; Zheng et al., 2007; Barratt et al., 2008; Zheng et al., 2009; Baka et al., 2011). The main idea of statistical model-based shape reconstruction is to find statistically plausible parameter values of the model that minimize a fitting criterion between the instantiated model and the available patient-specific information. Common to these works is the type of information used to guide the reconstruction, which consists of explicit morphological observations such as surface patches, contours or points. Such methods generally rely on multi-linear regression approaches. In (Liu et al., 2004a) canonical correlation analysis (CCA) was used to predict abnormal brain tissues from known correlations with other brain structures. In (Rao et al., 2008a, 2006) prediction of the morphology of brain structures was investigated based on the analysis of shape correlations amongst different structures in the brain and Partial Least Squares (PLS) Regression. In (Yang et al., 2008) a PLS based regression was also used to predict the humerus bone from surface points of the scapula. Extensions to non-linear constraints have been proposed for scene generation in the context of surgical simulators (Sierra et al., 2006; Harders and Székely, 2007; Basdogan et al., 2007). Though in these papers, the constraints are based on non-linear functions of point positions, these still refer to explicit shape landmarks. Such approaches do not consider anthropometric patient information such as height, weight or age which, although less explicitly related to the organs morphology, can also be expected to be relevant shape predictors.

* Corresponding author. Address: IMS Laboratory, University of Bordeaux, France.
E-mail addresses: rblanc33@gmail.com (R. Blanc), mauricio.reyes@istb.unibe.ch (M. Reyes).

1361-8415/$ - see front matter © 2012 Elsevier B.V. All rights reserved.
http://dx.doi.org/10.1016/j.media.2012.04.004

In (Rohlfing et al., 2009a,b) multi-linear regression is used to create an age-dependent brain atlas, therefore drawing an explicit link between age and brain morphometry. For a similar purpose, Ericsson et al. (2008) proposed to use non-parametric regression. In (Blanc et al., 2009) a non-parametric approach for conditional shape modeling was introduced, which enables to constrain a statistical model simultaneously by several anthropometric and morphometric information. The results highlight the more compact model that can be attained by conditioning the space of plausible shapes, making the proposed method suitable to create patient-specific shape models, while reducing the space of the modeled shape variability.

The aim of this paper is to compare different approaches capable of exploiting heterogeneous sources of information for the purpose of statistical model based shape prediction, and to investigate the added value of different types of predictors. We report results obtained using multivariate regression techniques for bone shape prediction using both anthropometric and morphological data constraints as well as explicit predictors, in the form of surface patches or points clouds directly observed from the surface of the organ, that are clinically and surgically relevant in the context of minimally invasive surgery. Different state of the art regression methods such as partial least square regression (PLS), principal component regression (PCA), canonical correlation analysis (CCA), and non-parametric kernel-based regression are compared on a database of 142 human femurs, and another of 154 human tibias. The prediction results are evaluated using leave-one-out cross validation.

Section 2 introduces the data, their preprocessing to generate a statistical shape model, and the set of morphological and anthropometric predictors considered in our experiments. Section 3 describes the generic shape prediction approach employed in this study, and the specific mathematical regression models we compare, specifically PLS, PCA, and CCA. Section 4 proposes several experiments to compare the different regression techniques, and the predictive value of various combinations of predictors. Finally, section 5 discusses the obtained results and concludes the paper.

2. Data and preprocessing

A total of 142 femurs and 154 tibias were selected from our database (age range: 23–83, mean 62.57 std. dev. 15; 46% males and 54% females) of CT scans, from individuals of known gender, age, height and weight. The images were acquired on a Toshiba Aquilion CT scanner, with a resolution of 0.877 mm and slice increments of 1 mm. The set of CT scans were initially pre-processed by semi-automatic segmentation using the Amira software (Mercury systems).

2.1. Point distribution model

In this study, image registration is used to provide a way to establish point correspondences amongst shapes in order to simultaneously generate the statistical shape model, extract the morphological parameters in a consistent way across the set of shapes, and build the regression functionals for shape prediction. The image registration pipeline is based on previous work focusing on high-throughput bone morphology assessment (Seiler et al., 2009). First, a common reference image is chosen from the cohort. Based on this selection, affine-based image registration is performed between the reference image and the remaining datasets (Ourselin et al., 2000). The aim of this step is to provide the non-rigid registration with an initialization for the final image warping. The underlying parameters were chosen empirically as three multi-resolution levels, 10 maximum number of iterations per level, normalized correlation coefficient metric, and tri-linear interpolation. The non-rigid registration we adopted is based on the work of (Vercauteren et al., 2008), where a diffeomorphic demons registration approach is proposed. In this registration framework the results of the registration are stationary velocity fields, which can be looked at as generators for diffeomorphic deformations, and efficiently computed using the scaling and squaring method (Arsigny et al., 2006). In addition, a femur-specific polyaffine regularization model was used to improve the accuracy of the non-rigid registration method. This regularization model is composed of a three-compartmental transformation covering the proximal, distal and shaft sections of the bone. During the log-domain optimization step, a linear-square problem is solved with respect to the velocity field to find the parameters of the polyaffine transformation used during regularization (Seiler et al., 2010). Similarly to the affine image registration, the selection of parameters for the non-rigid algorithm was chosen empirically as three multi-resolution levels, ten iterations per level, Gaussian regularization with standard deviation of 1 pixel, sum of square intensity differences as metric and tri-linear interpolation. After non-rigid registration, the resulting displacement vector fields are used to build a point distribution model (PDM) of the bone surface by propagating point-correspondences on the reference bone surface mesh. This propagation requires interpolation of displacement vector fields at each bone surface mesh node. Consequently, to ensure good correspondences at the bone surface, a labeled bone tissue image was used to enforce an anisotropic sampling of the displacement vector fields, where background-labeled voxels are excluded from the interpolation. In order to better take into account the effects of sparse observation on shape prediction and the uncertainties related to pose estimation, we proceed as in (Baka et al., 2010) by aligning all meshes to the reference with respect to the parts of the bone that will be observed. Finally, the built PDM is used to propagate morphological measurements defined on the reference bone over the cohort. The PDM and set of measurements are then used to build the shape regression functionals described in the following section.

2.2. Morphometric variables

The morphometric predictors were chosen according to commonly used clinically and surgically relevant parameters (Mahaisavariya et al., 2002; Rubin et al., 1992; Hitt et al., 2003; Tajima

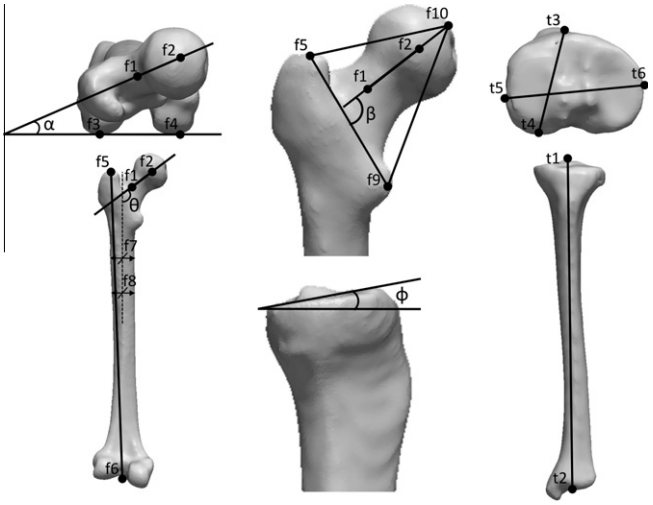

Fig. 1. Distance and angle based predictors for femur and tibia. Leftmost: proximal–distal (top) and anterior aspect (bottom) of the femur. Middle: Proximal anterior aspect of the femur (top), and proximal medial lateral tibia (bottom). Rightmost: proximal–distal and posterior aspect of the tibia.

Please cite this article in press as: Blanc, R., et al. Statistical model based shape prediction from a combination of direct observations and various surrogates: Application to orthopaedic research. Med. Image Anal. (2012), http://dx.doi.org/10.1016/j.media.2012.04.004

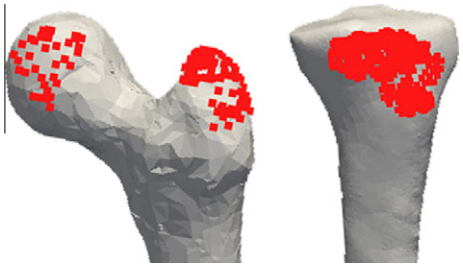

Fig. 2. Point clouds used to simulate US imaging as typically used in computer assisted orthopaedic surgery, see text for references. The point of clouds is later considered as predictor variable.

Table 1
Summary of predictor values for the population used in these experiments.

	Mean	SD	Max	Min
Femur				
Age (years)	63.89	16.23	93.00	21.00
Height (cm)	165.85	6.93	181.00	150.00
Weight (kg)	71.29	15.24	140.00	42.00
Femur length (mm)	413.63	22.70	474.19	352.19
Intercondyle distance (mm)	49.62	3.85	60.52	41.95
Neck length (mm)	63.65	5.15	75.50	50.32
Head diameter (mm)	46.78	3.59	55.88	39.28
Anteversion angle (°)	18.22	1.14	21.49	13.60
Collo-diaphysis angle (°)	129.82	5.37	141.38	116.46
Trochanter-neck angle (°)	90.88	4.08	99.53	80.57
Greater trochanter-head distance (mm)	69.19	5.40	85.24	58.35
Lesser trochanter-head distance (mm)	82.71	5.44	96.62	68.79
Tibia				
Age (years)	64.78	15.62	90.0	21.0
Height (cm)	166.16	6.81	181.00	151.00
Weight (kg)	71.82	15.23	140.00	42.00
Tibia length (mm)	352.59	21.37	401.21	299.05
Tibia plateau height (mm)	59.17	5.17	75.48	47.95
Tibia plateau slope (°)	15.21	2.30	23.12	10.08
Tibia plateau width (mm)	77.46	5.45	92.93	65.73

et al., 2009; Krebs et al., 2009; Parratte et al., 2008; Schünke et al., 2006). Fig. 1 summarizes distance and angle-based predictors, while Fig. 2 shows areas typically observed using US imaging to perform computer-assisted surgery (Mozes et al., 2010; Dekomien et al., 2007; Barratt et al., 2008; Schumann et al., 2010), which we will consider as potential shape predictors. The morphological predictors are defined in more detail in B and C.

Statistics of the distribution of the considered anthropometric and morphometric variables observed on our database are presented in Table 1. The correlation coefficient between pairs of variables are given in Fig. 3a) and Fig. 3b for femur and tibia, respectively.

3. Shape prediction

In practical applications such as navigation in minimally invasive surgery, and especially in the context of sparse observation of the shape surface, shape prediction involves two main steps: (1) the identification of the observed parts, which necessitate to draw correspondences between the observation and locations on the surface of the statistical shape model; and (2) the estimation of pose and shape parameters, which enables casting a patient specific instance of the statistical shape model in the coordinate system of the imaging system.

3.1. General approach

Methods such as the Iterative Closest Point (ICP) transform and its variants Besl and McKay (1992); Fleute and Lavallée (1998) can be employed to estimate correspondences. From an initial instance of the shape model, correspondences are obtained by matching the closest pairs of points between the observation data and the shape model. Then, shape and pose parameters are optimized to minimize the distance between corresponding pairs of points, and the process is iterated until convergence.

For the optimization of shape and pose parameters, we follow the approach proposed in Blanz et al. (2004), which consists in approximating the pose transform, so that the predicted shape can be expressed as a large linear system depending on both shape and pose parameters. The pose transformation is approximated through the estimation of pseudo-eigenvectors, which are concatenated to the modes of deformation of the statistical shape model.

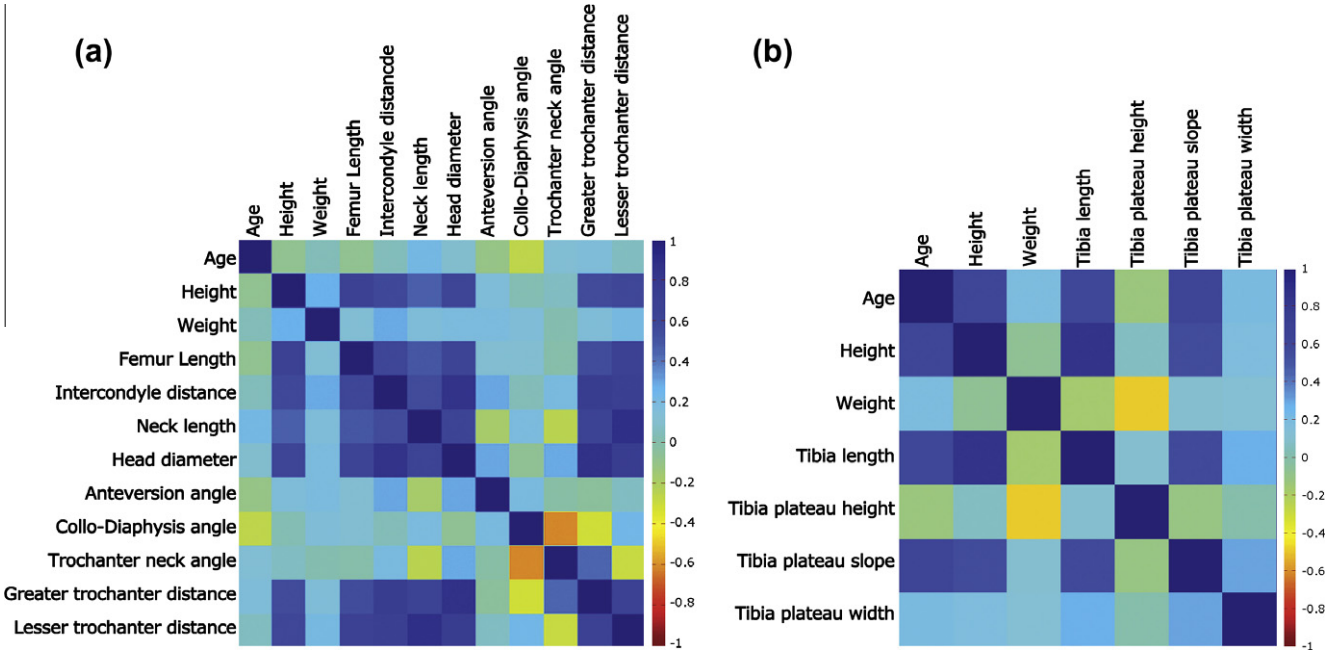

Fig. 3. Correlation coefficient calculated for the matrix of predictors measures for the femur (a) and tibia (b) shapes.

Please cite this article in press as: Blanc, R., et al. Statistical model based shape prediction from a combination of direct observations and various surrogates: Application to orthopaedic research. Med. Image Anal. (2012), http://dx.doi.org/10.1016/j.media.2012.04.004

Contrary to other methods that rely on alternated optimization of the shape and pose parameters separately, this approximation allows for the optimal parameters to be jointly estimated analytically in a single step, as the solution of a regularized multilinear regression model. This method involves an approximation of the rotation and possibly scaling components of the transform. However, this approximation remains reasonable when only small angles need to be corrected. Furthermore, as suggested in Blanz et al. (2004), larger corrections can be dealt with by iteratively applying the estimated pose to the mean shape and repeating the regression until convergence. While in Blanz et al. (2004), the authors propose to employ a regularized pseudo-inverse to perform the regression, the different regression schemes presented in the following section 3.2 can be employed as well.

The integration of morphometric and anthropometric predictors in these regression models will be discussed in Section 3.5. However, since these predictors are pose invariant by nature and do not depend on the establishment of correspondences with the model, it is appealing to exploit them by first computing a shape distribution conditioned on the values of these predictors, and then perform the actual shape regression using the observation data. We briefly describe a conditional Gaussian model, and a method based on kernel density estimation in Section 3.4. Additional comments on the implementation of the regression are given in A.

3.2. Multivariate statistical analysis for shape prediction

As mentioned in the introduction, the aim is to predict the shape of the complete organ of interest given various predictors. Let denote y the (column) vector of variables to predict, and x the available predictors. For these sets of variables, the statistical model provides a set of training samples, respectively denoted Y and X, from which we estimate the sample mean and covariance m_x, m_y, S_{xx}, S_{yy} The prediction of y from x can be performed using multivariate linear regression, as described in (Hastie et al., 2001 and Weisberg and January, 2005). In this study, three methods that have been employed in the context of statistical model based shape prediction will be investigated, namely regression based on Principal Component Analysis (PCA), also known as principal component regression, Partial Least Squares (PLS) and Canonical Correlation Analysis (CCA). A brief description of these techniques is given below, while more details can be found in (Borga et al., 1997; Muller, 1981/06/27; Hastie et al., 2001; Weisberg and January, 2005) and references therein. The principle of multivariate linear regression is to form an estimate.[1]

$$\hat{y} = B\dot{x} \tag{1}$$

A usual optimality criterion for B, is the Ordinary Least Squares (OLSs), which minimizes the Frobenius norm of the residuals on the training set:

$$R = \left\| \dot{Y} - \hat{\dot{Y}} \right\|_F^2 \Longleftrightarrow B^{(OLS)} = S_{yx}(S_{xx})^{-1} \tag{2}$$

However, in the context of statistical shape models, S_{xx} usually cannot be directly inverted due to both a limited number of observations and the presence of linear relations between the variables in x. One traditional way to deal with rank deficiency in S_{xx} is to add a regularization term, e.g. as in ridge regression through a small positive definite matrix, prior to the inversion: $B^{(OLS)} = S_{yx}(S_{xx} + \lambda I)^{-1}$, where λ is a ridge regression parameter to be optimized.

[1] Note that a dot on top of a variable indicates that it is centered: $\dot{x} = x - m_x$; it is also possible to estimate the intercept by replacing the vector $\dot{x}$ by $[1;\dot{x}]$ in (1), and modify the size of B accordingly.

3.3. Subspace methods for regression

Another possibility is to project the data in a subspace where it is not rank deficient, and calculate its inverse in this subspace. The different methods mentioned above differ by the choice of the subspace: PCA uses a projection in a subspace where $\dot{X}$ has a maximum variance, while PLS and CCA choose subspaces which maximize respectively the covariance and the correlation between $\dot{X}$ and $\dot{Y}$ (Borga et al., 1997; Liu et al., 2004b; Bennett et al., 2003).

3.3.1. Regression based on PCA

Using singular value decomposition $\dot{X} = UTV^T$ (Golub and Van Loan, 1996), the covariance matrix S_{xx} can be written as:

$$S_{xx} = \frac{1}{n-1} U\left(T^T T\right) U^T \tag{3}$$

The unitary matrix U contains the eigenvectors of S_{xx}, while the elements of the diagonal matrix $\frac{(T^T T)}{(n-1)}$ are its eigenvalues. As U forms an orthonormal basis, $U^{-1} = U^T$, the inverse of S_{xx} can be written:

$$S_{xx}^{-1} = (n-1)U\left(T^T T\right)^{-1} U^T. \tag{4}$$

If S_{xx} has small (or zero) eigenvalues, this inversion is clearly unstable (or not even defined). PCA avoids this problem by selecting only the r largest eigenvalues and their corresponding eigenvectors before inversion, that is keeping only the r first columns of U and T, in a way similar to the Moore–Penrose pseudo-inverse. However, r is considered here as a parameter of the regression that can be optimized.

The PCA regression coefficients are thus expressed as:

$$B^{(PCA)} = S_{xy}U_r\left(T_r^T T_r\right)^{-1} U_r^T, \tag{5}$$

where the basis U_r and the scores T_r are provided by the SVD decomposition of $\dot{X}$.

3.3.2. Regression based on partial least squares

In PLS, instead of finding the directions u_i where the variance of $\dot{X}$, or similarly $u_i^T \dot{X}\dot{X}^T u_i$, is maximum, the aim is to find pairs of directions u_i and v_i so that the covariance, and thus also $\rho_i = u_i^T \dot{X}\dot{Y}^T v_i$ is maximal, while still keeping the constraint that both $U_r = [u_1, \ldots, u_r]$ and $V_r = [v_1, \ldots, v_r]$ form orthonormal bases.

Taking the partial derivatives of ρ_i, setting them to zero and following the constraint that u_i and v_i are unitary vectors, it can be shown that those directions are obtained by resolving the following eigenvector problem:

$$\begin{aligned} S_{xy}S_{yx}u_i &= \rho_i^2 u_i \\ S_{yx}S_{xy}v_i &= \rho_i^2 v_i \end{aligned} \tag{6}$$

The scores T_r, and the final regression coefficients are then given by

$$\begin{aligned} T_r &= \dot{X}^T U_r \\ B^{(PLS)} &= S_{xy}U_r\left(T_r^T T_r\right)^{-1} U_r^T \end{aligned} \tag{7}$$

3.3.3. Regression based on canonical correlation analysis

In the case of CCA, pairs of directions producing maximum correlations are sought:

$$\rho_i = \frac{u_i^T S_{xy} v_i}{\sqrt{u_i^T S_{xx} u_i v_i^T S_{yy} v_i}} \tag{8}$$

Maximizing with respect to u_i and v_i leads to a generalized eigenvalue problem:

$$\begin{aligned} S_{xy}S_{yy}^{-1}S_{yx}u_i &= \rho_i^2 S_{xx}u_i \\ S_{yx}S_{xx}^{-1}S_{xy}v_i &= \rho_i^2 S_{yy}v_i, \end{aligned} \tag{9}$$

Please cite this article in press as: Blanc, R., et al. Statistical model based shape prediction from a combination of direct observations and various surrogates: Application to orthopaedic research. Med. Image Anal. (2012), http://dx.doi.org/10.1016/j.media.2012.04.004

where the matrices on both sides are symmetric. Though S_{xx} and S_{yy} are generally only semi-definite positive, a good approximation can be obtained, as previously, by adding a small positive matrix before inversion. Another solution is to perform a PCA on S_{xx} first, and retain only the eigenvalues which are not too close to zero.

Retaining the directions U_r corresponding to the principal modes defined by (8) and pluging them in equation (7) leads to the corresponding coefficients B^{CCA}.

3.4. Conditional models

Another way to look at shape prediction is to consider the joint distribution of both predictors and variables to predict, $P(x,y)$, and to calculate the conditional distribution $P(y|x)$ describing a conditional model of the shape given these predictors values. In particular, the conditional expectation $E[y|x]$ can be considered as an estimate of the shape that best corresponds to the observed predictors. Two different models for the joint distribution $P(x,y)$ are considered here: a simple multivariate Gaussian model, and the kernel density model proposed in (Blanc et al., 2009).

3.4.1. Multivariate normal model

This model is characterized by two parameters, the mean m and covariance matrix S of the normal distribution, which we estimate through the sample statistics, i.e.:

$$m = [m_x; m_y]; \quad S = \begin{pmatrix} S_{xx} & S_{xy} \\ S_{xy}^T & S_{yy} \end{pmatrix} \tag{10}$$

Under this model, the conditional mean is expressed as:

$$\hat{y} = E[y|x] = m_y + S_{xy}S_{xx}^{-1}(x - m_x), \tag{11}$$

which is equivalent to the OLS regression. The same considerations related to the inversion of S_{xx} apply, as well as the possibility to add a regularization term to S_{xx} to stabilize its inversion, at the cost of a small bias in $E[y|x]$.

The full conditional distribution is also Gaussian, with covariance:

$$Cov[y|x] = S_{yy} - S_{xy}S_{xx}^{-1}S_{xy}^T, \tag{12}$$

Since this is a Gaussian model, the conditional distribution can be safely expressed through a mean shape $E[y|x]$ and a set of linear deformations obtained from the diagonalization of $Cov[y|x]$.

3.4.2. Kernel density model

A kernel density model is a non-parametric method for estimating a probability distribution from a set of samples. It relies on the choice of a kernel function K_H, where H is the kernel bandwidth. We choose a Gaussian kernel, and optimize its bandwidth through cross-validation as proposed in (Blanc et al., 2009).

$$P(y,x) = \frac{1}{n}\sum_{i=1}^{n} K_H(y - y_i, x - x_i) \tag{13}$$

$$\hat{y} = E[y|x] = \sum_{i=1}^{n} w_i \mu_{y|x}^{(i)} \tag{14}$$

with $w_i = \frac{K_{H_x}(x-x_i)}{\sum_{j=1}^{n} K_{H_x}(x-x_j)}$ and $\mu_{y|x}^{(i)} = y_i + W_{yx}W_{xx}^{-1}(x - x_i)$.

Since this distribution model is non linear, the conditional distribution obtained by this approach cannot be directly plugged in the statistical model based shape prediction described in 3.1. The proposed two-step shape estimation is therefore not recommended with the shape fitting techniques described in this paper, and only the conditional shape $E[y|x]$ given both the observation data and patient meta-information will be considered in the experiments.

3.5. Incorporation of anthropometric and morphometric predictors

Scalar predictors (i.e. continuous variables) such as the morphometric and anthropometric parameters described in Section 2.2 can directly be incorporated into these regression schemes, concatenating them into the vector x of predictors (response matrix X of training data). However, due to the typically large number of point predictors compared to anthropometric and morphometric variables, it may be preferable to pay special attention to the balance between the different types of predictors. This can be achieved for instance by re-scaling the different variables. In our experiments, we replaced the point predictors by their projection in the corresponding PCA space characterized by m_x and S_{xx}, effectively reducing the number of surface-related predictors, and directly concatenated them with the continuous anthropometric and morphometric predictors. In extenso, the vector of predictors is written:

$$x = \begin{pmatrix} p_{pts} \\ x_{meta} \end{pmatrix} \tag{15}$$

where x_{meta} is the vector of anthropometric and morphometric predictors, and p_{pts} a compact representation of the point predictors.

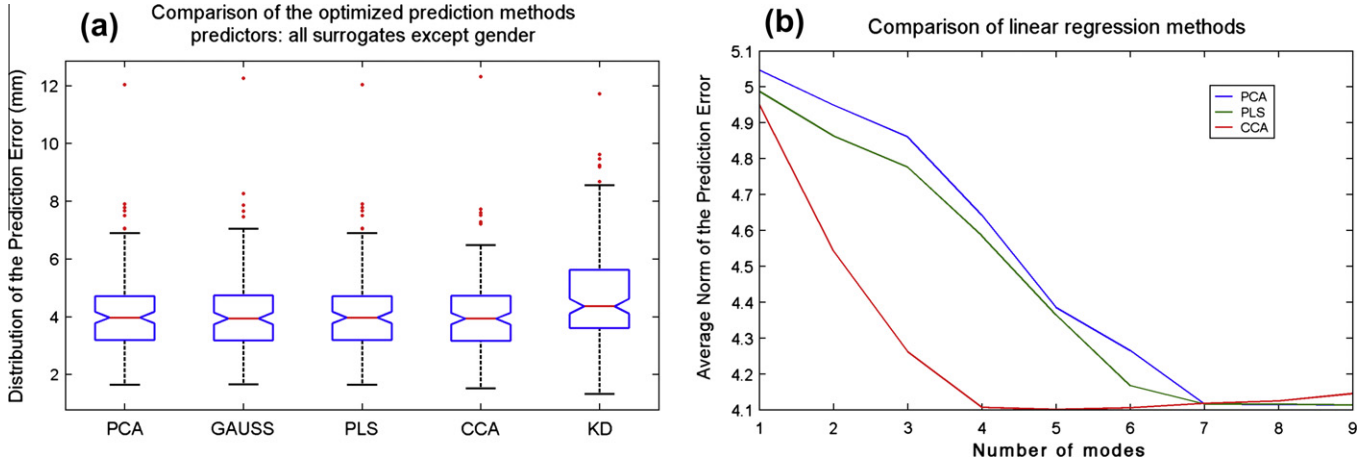

Fig. 4. (a) Influence of the dimensionality reduction on the average prediction errors for PCA, PLS and CCA regression methods. (b) Distribution of the prediction error after optimization of prediction parameters. Results obtained with the femur model and all available surrogate variables as predictors.

Please cite this article in press as: Blanc, R., et al. Statistical model based shape prediction from a combination of direct observations and various surrogates: Application to orthopaedic research. Med. Image Anal. (2012), http://dx.doi.org/10.1016/j.media.2012.04.004

In the case of categorical predictors, such as the gender or ethnic group, a straightforward solution is to train a statistical model using only the adequate subset of training samples, provided that enough cases in an available database comply with the given constraints.

4. Experimental study

We propose three experiments to investigate different aspects related to shape prediction from various types of predictors. In a first experiment, we compare the performances of the different regression techniques presented in Section 3.3 using a fixed combination of predictors from the set of sparse surface observations, anthropometric and morphometric measurements defined in Section 2.2. A second experiment compares the accuracy of shape prediction using different sets of predictors. For both experiments, in order to simplify the comparisons and to concentrate exclusively on shape differences, the exact pose and correspondences are used. In a third experiment, we analyze in more details the interest of using anthropometric information to complement sparse observations in a complete shape fitting experiment, including the estimation of shape and pose, as well as correspondences between the sparse observation and the shape model.

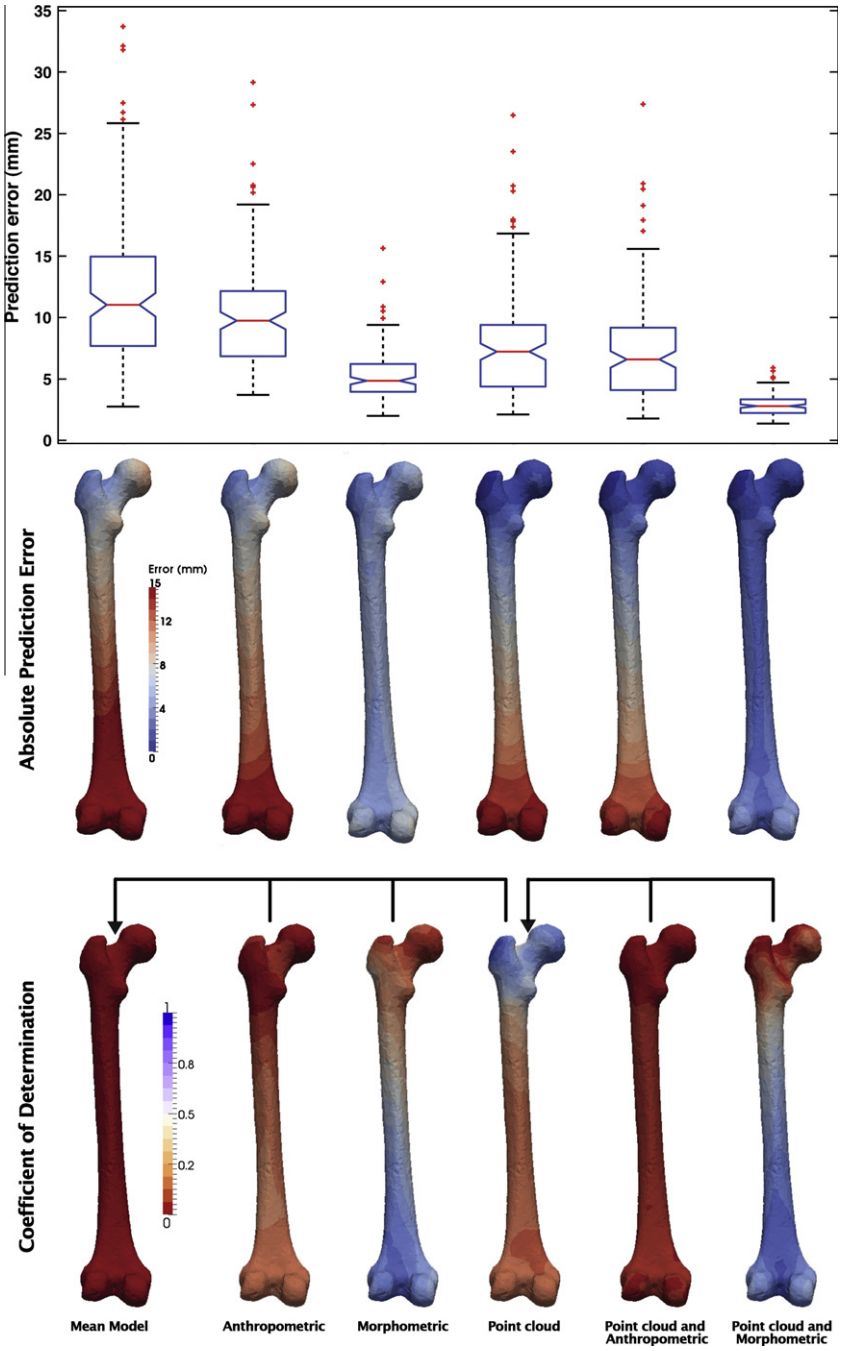

Fig. 5. Summary of prediction errors for different sets of predictors. Top: Whisker plots of mean prediction errors. Middle: Color-coded absolute average prediction error. Bottom: Coefficient of determination relative to the mean shape model variability and point-cloud-based prediction. Arrows indicate the base prediction used as reference (please refer to main text). Values close to 0 indicate low variability reduction of the prediction over the population, whereas values close to 1 indicate a strong reduction of the variability. From left to right, mean shape, anthropometric, morphometric information, point cloud (surface points), point cloud plus anthropometric, point cloud plus morphometric information. (For interpretation of the references to color in this figure legend, the reader is referred to the web version of this article.)

Please cite this article in press as: Blanc, R., et al. Statistical model based shape prediction from a combination of direct observations and various surrogates: Application to orthopaedic research. Med. Image Anal. (2012), http://dx.doi.org/10.1016/j.media.2012.04.004

In all the experiments, for both the femur and tibia models, a systematic leave-one-out (LOO) cross validation is performed to estimate the optimal values for the parameters of the various regression methods described in Section 3.2, and to evaluate the corresponding prediction accuracy. For each predicted shape, we compute the point-wise prediction error as the distance between each predicted point and its ground-truth counterpart, using a shape model trained on all other available shapes. The average prediction error, computed over all points and all predicted shapes in the LOO experiment, is used as the goal function for the optimizations.

4.1. Comparison of shape regression methods

In this experiment, we exploit the full set of anthropometric and morphometric predictors described in Section 2.2, except gender, to compare the regression methods presented in Section 3.2.

As can be seen in Fig. 4a, the different linear methods appear to perform in a very similar way, after optimization of both the number of retained dimensions and of the coefficient of the regularization term. Rather than in the estimated optimum, the differences between the prediction methods mostly appear in their behavior with respect to the number of retained modes, as shown in Fig. 4b. Namely, PLS and in particular CCA manage to capture most of the relations between the predictors and the predicted shape with fewer modes compared to PCA. However, the computational cost associated to CCA hinder its use in large-scale experiments. Not surprisingly, the conditional mean under the Gaussian model prove to generate results very similar to the linear regression approaches. However, rather unexpectedly, the kernel density approach appeared to provide less accurate estimations. We believe this is due to the difficulties related to bandwidth selection in such a sparsely sampled, high dimensional space.

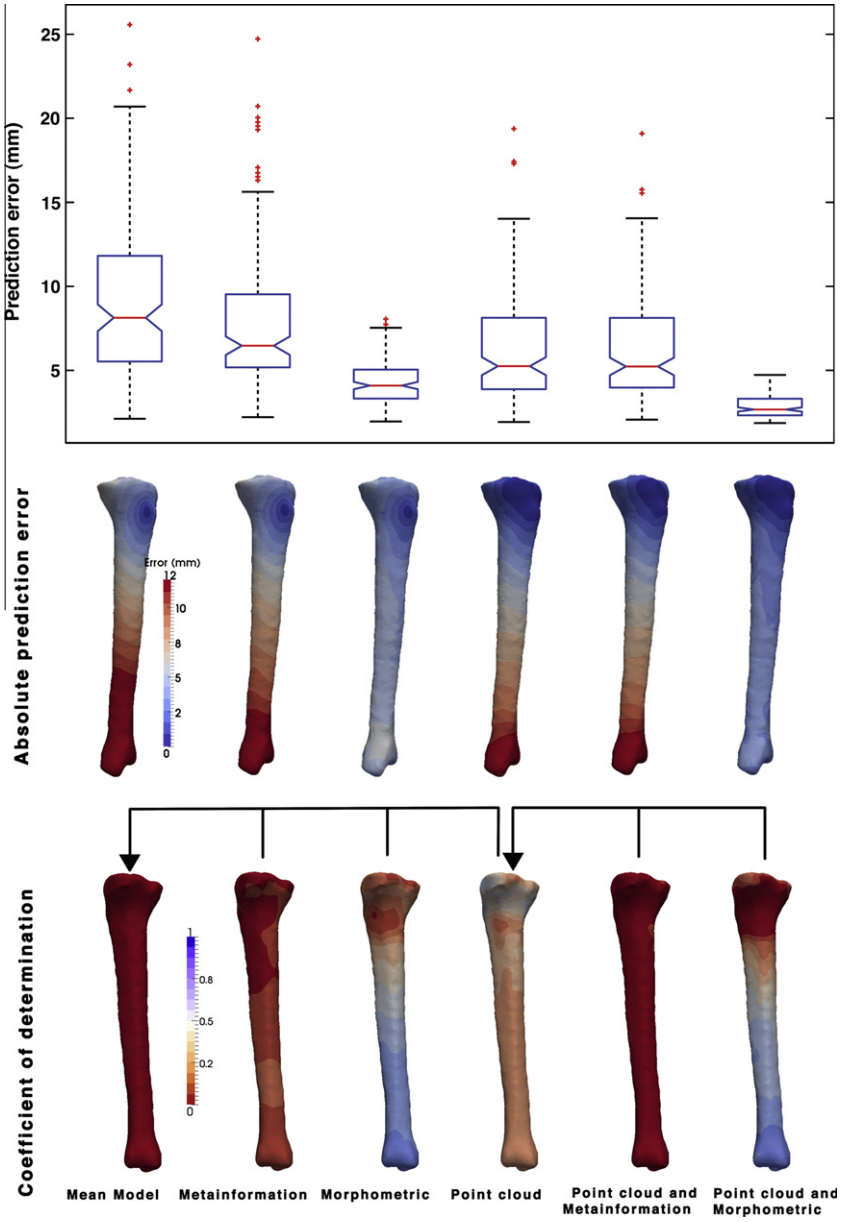

Fig. 6. Summary of prediction errors for different sets of predictors. Top: Whisker plots of mean prediction errors. Middle: Color-coded absolute average prediction error. Bottom: Coefficient of determination relative to the mean shape model variability and point-cloud-based prediction. Arrows indicate the base prediction used as reference. Values close to 0 indicate low variability reduction of the prediction over the population, whereas values close to 1 indicate a strong reduction of the variability. From left to right, mean shape, anthropometric, morphometric information, point cloud (surface points), point cloud plus anthropometric, point cloud plus morphometric information. (For interpretation of the references to color in this figure legend, the reader is referred to the web version of this article.)

Please cite this article in press as: Blanc, R., et al. Statistical model based shape prediction from a combination of direct observations and various surrogates: Application to orthopaedic research. Med. Image Anal. (2012), http://dx.doi.org/10.1016/j.media.2012.04.004

A similar behavior was observed with different combinations of predictors, both on the femur and tibia models. Therefore, in the following, we only report the results corresponding to the simpler and faster PCA method.

4.2. Shape estimation using different sets of predictors

In this experiment, we investigate the influence of the different predictors on the shape prediction accuracy in a more localized fashion by computing the average prediction error at each shape point. We compare the LOO variability using:

1. No predictors (generalization ability of the SSM).
2. Anthropometric predictors only.
3. Morphometric information only.
4. Surface information only.
5. Surface information and anthropometric predictors.
6. Surface information, anthropometric and morphometric predictors.

Furthermore, in order to gain a better understanding of the complementarity or redundancy of the various predictors being considered, the variances of the point-wise prediction error distributions observed using different combinations of predictors are compared. The following ratio allows us to directly quantifies their relevance in a localized fashion:

$$D = 1 - \frac{var(\widehat{Y}_X - Y)}{var(\widehat{Y}_R - Y)}, \tag{16}$$

with $var(\cdot)$ the variance operator and $\widehat{Y}_X$ the predicted shape using predictor set X, $\widehat{Y}_R$ the prediction obtained using a reference predictor R. When no predictor is used, $\widehat{Y}_R$ is replaced by the mean model m_Y, and D corresponds to the coefficient of determination. Equation (16) reflects a low relevance of the predictor set $\widetilde{X}$ with respect to the reference variance when D is low, and high predictive value of the predictor set when it is close or equal to 1.

The summary of the prediction errors for both models, and for various combinations of predictors are presented in Figs. 5 and 6. On the first row, the distribution of the prediction errors (after optimization of the parameters of the regression methods) are displayed. The meshes on the second row show the localized, point-wise average prediction error, while the third row shows the reduction of uncertainty allowed by the corresponding predictors. These figures illustrate how localized the effects of the different predictors are, and especially how the information can be combined to improve the prediction accuracy. On each figure, the arrow pointing from experiment i to experiment j indicates that the experiment j is taken as the baseline for computing the coefficient of determination and is therefore used as the denominator in (16). For example, compared to using point cloud information alone, the utilization of both point cloud and anthropometric predictors does not result in significant improvements.

4.3. Shape fitting

Finally, we consider the complete problem of shape fitting, including the estimation of correspondences between the observation data and the shape model, and the pose and shape parameters. For correspondence establishment, we use an ICP algorithm between the observation point cloud and a subset of the shape model, restricted around the femur head and neck to add some constraints to the problem. When anthropometric is used, we first compute the conditional shape distribution given the anthropometric data (gender, height, age and weight), using the multivariate Gaussian model described in Section 3.4.1, and apply the shape fitting algorithm.

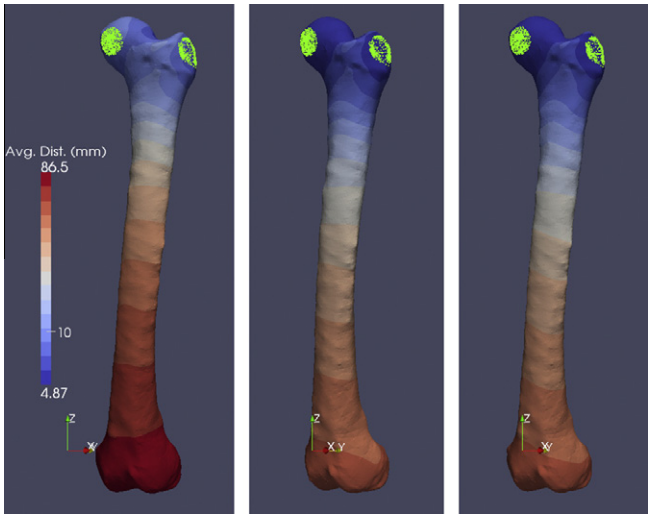

Fig. 7. Example of shape fitting results (C0) using only the sparse observation data represented by the green dots on the images, (C1) using gender, height, age and weight information, (C2) using height, age, weight and intercondyle distance. The direct comparison of shapes is made difficult due to uncertainties in the estimation of the rotation parameters. (For interpretation of the references to color in this figure legend, the reader is referred to the web version of this article.)

Table 2
General quality metrics, and shape specific ones. For the latter, both the average error and the Pearson correlation coefficient are given. (C0) using only the sparse observation data represented by the green dots on the images, (C1) using gender, height, age and weight information, (C2) using height, age, weight and intercondyle distance.

	C0	C1	C2
Average distance	43.05 mm	28.32 mm	35.76 mm
Standard deviation	29.2	18.8	24.3
Femur length	−16.0 mm ($R = 0.31$)	−0.4 mm ($R = 0.74$)	−7.5 mm ($R = 0.61$)
Intercondyle distance	−4.2 mm ($R = 0.05$)	−1.6 mm ($R = 0.45$)	0.11 mm ($R = 0.99$)
Neck length	−1.7 mm ($R = 0.42$)	0.17 mm ($R = 0.74$)	−0.38 m ($R = 0.64$)
Head diameter	−2.4 mm ($R = 0.52$)	−0.91 mm ($R = 0.70$)	−1.6 mm ($R = 0.69$)
Neck/shaft angle	−4.1° ($R = 0.16$)	−1.0° ($R = 0.27$)	−2.3° ($R = 0.26$)
Anteversion angle	1.7° ($R = 0.21$)	0.95° ($R = 0.33$)	0.99° ($R = 0.19$)

Since the observation data we use are very sparse (see Fig. 2), large errors can be expected on the rotational components of the pose estimation. Indeed, when the observations are restricted to one end of an elongated shape, small errors in the estimation of the rotation lead to large errors in shape parts far away from any observation, as can be observed in Fig. 7. Therefore, in addition to the point-wise prediction error, we also evaluate the morphological measurements described in Section 2.2 and consider them as pose-independent goodness-of-fit measures. The results in Table 2 indicate that a significant improvement is obtained in terms of shape fitting when complementing the sparse observation data with additional information, in terms both of general and shape specific metrics. Note that for experiment C2, the intercondyle distance is used both as a predictor and a control variable. However, the control value is measured by the distance f3–f4 (see Fig. 1), which is not directly enforced by the regression. Indeed, the shape prediction method only relies on the statistical relationship between the surrogate variable and the shape model,

Please cite this article in press as: Blanc, R., et al. Statistical model based shape prediction from a combination of direct observations and various surrogates: Application to orthopaedic research. Med. Image Anal. (2012), http://dx.doi.org/10.1016/j.media.2012.04.004

following dimensionality reduction. The very high accuracy and correlation observed in this experiment can therefore be viewed as a measure of the quality of the statistical shape model and of the regression method employed.

5. Discussion and conclusions

On a methodological point of view, none of the regression approaches investigated here showed a clear benefit compared to the others in terms of prediction error. Relying on CCA, fewer modes were necessary to perform accurate predictions, but the additional computational burden clearly plays against this approach. Finally, the comparison with the non-linear kernel regression tends to indicate that it remains safer to stick to simpler models, at least unless more specific information is available for guiding the estimation of non-linear model or more data is available.

As can be seen on both Figs. 5 and 6, especially the coefficient of determination on the third row, a progressive improvement in the prediction is observed when adding more predictors, indicating that they bring complementary information. The locality of the information is clearly displayed. Obviously, point predictors bring much information about the areas in the vicinity of these points. However, for the type of point predictors considered here, not much information is gained about more distant locations. On the contrary, anthropometric predictors and especially the patient height, have a more global effect, due its correlation with the highly variable bone length. Morphometric information proved to be highly valuable, acting directly on specific and localized aspects of the bone morphology, and can potentially provide rich complementary information compared to the point predictors alone.

The localized coefficient of determination appears as an effective mean to easily display the added value of particular predictors or combinations of them. We believe it can be an efficient tool for investigating precisely which predictors are worth measuring for a specific application, like planning a specific minimally-invasive intervention in which limited intra-operative data may be acquired. However, since it is based on the variability of the shape model, which does not incorporate any uncertainty related to the position of the model, this statistics cannot be used for the investigation of complete shape fitting experiments as in Section 4.3.

The last experiment confirms that, even when very sparse observation data are available to guide the shape fitting, the exploitation of additional information such as anthropometric data proves very relevant. While the observation data leave substantial uncertainty on the pose parameters, as illustrated in Fig. 7 by the poor accuracy in the knee area, both the average prediction error and the pose-independent morphometric measures indicate a significant improvement when using this additional data. Since such data are easily accessible, we advocate that they should be systematically collected and exploited when constructing and utilizing statistical shape models.

Acknowledgment

The authors thank the National Center of Competence in Research, Computer-Aided and Image-Guided Medical Interventions (NCCR Co-Me), supported by the Swiss National Science Foundation (SNSF).

Appendix A. Practical implementation of the regression techniques

The operations required for performing eigenvalue decomposition or generalized eigenvalues decomposition can present high computational and memory costs when the dimensionality of the shape becomes large and tend to become unstable. Taking advantage of the SVD, PCA can be performed efficiently. Algorithms such as NIPALS or SIMPLS (de Jong and March, 1993) also exist, and allow an iterative resolution of eigenvalues problem, which also allow to keep the computational burden affordable for large models (Hubert and Branden, 2003). Unfortunately, no such fast and robust algorithm was found in the literature concerning CCA. In the context of statistical models, a number of papers (Rao et al., 2008b; Liu et al., 2004b) suggest to perform PLS or CCA after an initial PCA based dimensionality reduction of both X and Y. This means that the data matrices X and Y are replaced by (much smaller) matrices of parameters $\widetilde{X}$ and $\widetilde{Y}$ approximating them. It is clear that after retaining only the singular values of X which are sufficiently large, the covariance matrix $\widetilde{X}\widetilde{X}^T/(n-1)$ will be of full rank, and an OLS regression is then possible. Applying one of the subspace methods above can then only be interpreted as filtering remaining noise. The theoretical benefits of PLS or CCA may also be lost since this initial dimensionality reduction is performed without any regard to the statistical dependences between X and Y. We therefore recommend, if this first dimensionality reduction step is necessary, to keep the maximum number of dimensions in the initial PCA (usually n-1, where n is the number of training samples, e.g. using the "economy" size SVD of the data), before using PLS or CCA. For all the methods above, we optimized the number r of retained modes. Additionally, an additional regularization parameter λ was introduced whenever a matrix needed to be inverted, by replacing $(T_r^T T_r)^{-1}$ by $(T_r^T T_r + \lambda I)^{-1}$, so as to get an easy comparison with ridge regression. This parameter was also optimized. In order to get more insight on the influence of r and λ, a simple grid search optimization was employed. All optimizations were carried out using systematic leave-one-out experiments. The function actually being optimized, was the average distance between every point of the predicted shape to its true counterpart. In the case where the predictors contained points of the shape, we predicted only the missing points. The final shape was formed by using both observed and predicted points, and projecting the result within the original space of the statistical shape model. Whenever gender was used as a predictor, the training matrices X and Y were replaced by the corresponding subset of training samples sharing the same gender. Kernel regression was performed as described in (Blanc et al., 2009), using the conditional expectation as the predicted shape. Finally, we compared the results with those obtained by calculating the conditional distribution assuming a joint Gaussian distribution between the predictors and the shape.

Appendix B. Definition of morphological surrogate variables for Femur

The frontal and transversal planes are commonly created to aid the definition of landmarks (Schünke et al. (2006)).

Frontal plane: passing through the two most posterior points of the medial and lateral condyles (Fig. 1, f3 and f4) and the most posterior point of the lesser Trochanter (Fig. 1, f9).

Transversal plane: Perpendicular to the femur frontal plane and passing through the two most distal points on the medial and lateral Condyles.

- Bone Length. Bone length is defined as the distance between the most proximal point of the great trochanter (Fig. 1-f5) and the intersection point (see Fig. 1-f6) between the axis perpendicular to the transversal plane and passing across the head center (Fig. 1-f2), and the transversal plan.
- InterCondyle Distance (ICD). The inter-condyle distance is defined as the distance between the two most posterior points on the medial and lateral condyles (see Fig. 1, f3–f4).

Please cite this article in press as: Blanc, R., et al. Statistical model based shape prediction from a combination of direct observations and various surrogates: Application to orthopaedic research. Med. Image Anal. (2012), http://dx.doi.org/10.1016/j.media.2012.04.004

- Neck Length. The neck length is defined as the distance between the most medial and lateral points of the caput femoris axis, which is defined as the intersection of the head center (Fig. 1-f2) and the femoral neck center (Fig. 1-f1).
- Caput Collum Diaphysis (CCD) angle (θ). The angle of the caput femoris relative to the femoral proximal axis, projected on the frontal plane. The femoral proximal axis is defined as the intersection of the middle points at 2/10ths and 3/10ths of the femur length (Fig. 1, f7 and f8, respectively).
- Neck Anteversion Angle (α). It describes the angle of the caput femoris (Fig. 1, f1–f2) relative to the frontal plane (Fig. 1, f3–f4), projected on the transversal plane.
- Neck-Trochanter line angle (β). Angle relative to the frontal plane between the femoral neck line and the major and lesser trochanter line. See (Fig. 1, f1–f2).
- Trochanter-Fovea distances. The distances between the major and lesser trochanter to the fovea capitus. See Fig. 1, f5–f10 and Fig. 1, f9–f10, respectively.

Appendix C. Definition of morphological surrogate variables for Tibia

The frontal and transversal planes are commonly created to aid the definition of landmarks (Schünke et al. (2006)).

Frontal plane: passing through the two most posterior points of the medial and lateral condyles (Fig. 1-t4 and corresponding medial point) and the most posterior point of the distal tibia.

Transversal plane: Perpendicular to the tibia frontal plane and passing through the two most medial–lateral points on the medial and lateral tibial condyles, respectively (Fig. 1, t5–t6).

- Tibia Length. The tibia length is defined as the distance between the most superior point on tibia (Eminentia intercondylaris, Fig. 1-t1) and the center point of the ankle from the facies articularis inferior (Fig. 1-t2).
- Plateau Height. The plateau height is defined as the distance between the most anterior point to the most posterior point on the tibia plateau (Fig. 1, t3–t4).
- Plateau Width. The plateau width is defined as the distance between the most medial point and the most lateral point on the tibia plateau. (Fig. 1, t5–t6).
- Plateau Slope (Φ). Angle from the line connecting the medial and lateral tibial condyle to a plane perpendicular to the transversal plane.

References

Arsigny, V., Commowick, O., Pennec, X., Ayache, N., 2006. A log-euclidean framework for statistics on diffeomorphisms. In: Medical Image Computing and Computer-Assisted Intervention – MICCAI. pp. 924–931. <http://dx.doi.org/10.1007/11866565_113>.

Baka, N., de Bruijne, M., Reiber, J., Niessen, W., Lelieveldt, B., 2010. Confidence of model based shape reconstruction from sparse data. In: Biomedical Imaging: From Nano to Macro, 2010 IEEE International Symposium on. IEEE, pp. 1077–1080.

Baka, N., Kaptein, B.L., de Bruijne, M., van Walsum, T., Giphart, J.E., Niessen, W.J., Lelieveldt, B.P.F., 2011. 2d–3d Shape reconstruction of the distal femur from stereo X-ray imaging using statistical shape models. Med. Image Anal. 15 (6), 840–850.

Barratt, D.C., Chan, C.S., Edwards, P.J., Penney, G.P., Slomczykowski, M., Carter, T.J., Hawkes, D.J., 2008. Instantiation and registration of statistical shape models of the femur and pelvis using 3d ultrasound imaging. Med. Image Anal. 12 (3), 358–374.

Basdogan, C., Sedef, M., Harders, M., Wesarg, S., 2007. Vr-based simulators for training in minimally invasive surgery. IEEE Comput. Graph Appl. 27 (2), 54–66.

Benameur, S., Mignotte, M., Parent, S., Labelle, H., Skalli, W., de Guise, J., 2003. 3D/2D registration and segmentation of scoliotic vertebrae using statistical models. Comput. Med. Imag. Graph. 27, 321–337.

Bennett, K.P., Bennett, K.P., Embrechts, M.J., Embrechts, M.J., 2003. An optimization perspective on kernel partial least squares regression. In: Advances in Learning Theory: Methods, Models and Applications. Press, pp. 227–250.

Besl, P., McKay, N., 1992. A method for registration of 3-d shapes. IEEE Transactions on Pattern Analysis and Machine Intelligence 14 (2), 239–256.

Blanc, R., Reyes, M., Seiler, C., Székely, G., 2009. Conditional variability of statistical shape models based on surrogate variables. Medical Image Computing and Computer-Assisted Intervention – MICCAI 2009, vol. 5762. Springer, Berlin, Heidelberg, pp. 84–91.

Blanz, V., Mehl, A., Vetter, T., Seidel, H.-P., 2004. A statistical method for robust 3d surface reconstruction from sparse data. In: 3D Data Processing Visualization and Transmission, International Symposium on, pp. 293–300.

Borga, M., Landelius, T., Knutsson, H., 1997. A unified approach to PCA, PLS, MLR and CCA. Report LiTH-ISY-R-1992, ISY, SE-581 83 Linköping, Sweden.

Brenner, D.J., Hall, E.J., 2007. Computed tomography – an increasing source of radiation exposure. New Engl. J. Med. 357, 2277–2284.

Chan, C.S.K., Edwards, P.J., Hawkes, D.J., 2003. Integration of ultrasound-based registration with statistical shape models for computer-assisted orthopaedic surgery. In: Sonka, M., Fitzpatrick, J.M. (Eds.), Proc. SPIE Medical Imaging, vol. 5032. SPIE, pp. 414–424.

de Jong, S., 1993. Simpls: an alternative approach to partial least squares regression. Chemometr. Intell. Lab. Syst. 18 (3), 251–263.

Dekomien, C., Hold, S., Hensel, K., Schmitz, G., Winter, S., 2007. Registration of intraoperative 3d ultrasound with preoperative mri data for navigated surgery – first results at the knee. In: 7th Annual Meeting of the International Society for Computer Assisted Orthopaedic Surgery, Heidelberg, Germany. pp. 133–136.

Ericsson, A., Aljabar, P., Rueckert, D., 2008. Construction of a patient-specific atlas of the brain: application to normal aging. In: IEEE International Symposium on Biomedical Imaging. pp. 480–483.

Fleute, M., Lavallée, S., 1998. Building a complete surface model from sparse data using statistical shape models: application to computer assisted knee surgery.

Fleute, M., Lavallée, S., Desbat, L., 2002. Integrated approach for matching statistical shape models with intra-operative 2d and 3d data. Med. Image Comput. Comput. – Assist. Intervent. – MICCAI 2002, 364–372.

Fleute, M., LavallÈe, S., Julliard, R., 1999. Incorporating a statistically based shape model into a system for computer-assisted anterior cruciate ligament surgery. Med. Image Anal. 3 (3), 209–222.

Golub, G., Van Loan, C., 1996. Matrix Computations (Johns Hopkins Studies in Mathematical Sciences), third ed. The Johns Hopkins University Press.

Harders, M., Székely, G., 2007. Using statistical shape analysis for the determination of uterine deformation states during hydrometra. Med. Image Comput. Comput. Assist. Intervent. 10 (Pt 2), 858–865.

Hastie, T., Tibshirani, R., Friedman, J., 2001. The elements of statistical learning. In: Data Mining, Inference, and Prediction, . second ed.. Springer Series in Statistics second ed. Springer, New York.

Heimann, T., Meinzer, H.-P., 2009. Statistical shape models for 3d medical image segmentation: a review. Med. Image Anal. 13 (4), 543–563.

Hitt, K., Shurman, J.R. n., Greene, K., McCarthy, J., Moskal, J., Hoeman, T., Mont, M.A., 2003. Anthropometric measurements of the human knee: correlation to the sizing of current knee arthroplasty systems. J. Bone Joint Surg. Am., 115–122.

Hubert, M., Branden, K.V., 2003. Robust methods for partial least squares regression. J. Chemometr. 17 (10), 537–549.

Krebs, V., Incavo, S.J., Shields, W.H., 2009. The anatomy of the acetabulum: what is normal? Clin. Orthopaed. Relat. Res. 467 (4), 868–875.

Lamecker, H., Wenckebach, T.H., Hege, H.-C., 2006. Atlas-based 3d-shape reconstruction from X-ray images. In: ICPR '06: Proceedings of the 18th International Conference on Pattern Recognition. IEEE Computer Society, Washington, DC, USA, pp. 371–374.

Liu, T., Shen, D., Davatzikos, C., 2004a. Predictive modeling of anatomic structures using canonical correlation analysis. In: IEEE International Symposium on Biomedical Imaging: Nano to Macro, 2004. pp. 1279–1282.

Liu, T., Shen, D., Davatzikos, C., 04 2004b. Predictive modeling of anatomic structures using canonical correlation analysis. In: IEEE International Symposium on Biomedical Imaging: Nano to Macro – ISBI. pp. 1279–1282. <http://dx.doi.org/10.1109/ISBI.2004.1398779>.

Mahaisavariya, B., Sitthiseripratip, K., Tongdee, T., Bohez, E.L.J., Vander Sloten, J., Oris, P., 2002. Morphological study of the proximal femur: a new method of geometrical assessment using 3-dimensional reverse engineering. Med. Eng. Phys. 24 (9), 617–622.

Mozes, A., Chang, T.-C., Arata, L., Zhao, W., 2010. Three-dimensional a-mode ultrasound calibration and registration for robotic orthopaedic knee surgery. Int. J. Med. Robot. 6 (1), 91–101.

Muller, K., 1981/06/27. Relationships between redundancy analysis, canonical correlation, and multivariate regression. Psychometrika 46 (2), 139–142, <http://dx.doi.org/10.1007/BF02293894>.

Ourselin, S., Roche, A., Prima, S., Ayache, N., 2000. Block matching: a general framework to improve robustness of rigid registration of medical images. Med. Image Comput. Comput. – Assist. Intervent. – MICCAI 2000, CH373–CH373.

Parratte, S., Kilian, P., Pauly, V., Champsaur, P., Argenson, J.N.A., 2008. The use of ultrasound in acquisition of the anterior pelvic plane in computer-assisted total hip replacement: a cadaver study. J. Bone Joint Surg. Brit. 90 (2), 258.

Raisz, L.G., 2005. Clinical practice. Screening for osteoporosis. New Engl. J. Med. 353, 164–171.

Rajamani, K.T., Styner, M.A., Talib, H., Zheng, G., Nolte, L.P., Ballester, M.A.G., 2007. Statistical deformable bone models for robust 3d surface extrapolation from sparse data. Med. Image Anal. 11 (2), 99–109.

Please cite this article in press as: Blanc, R., et al. Statistical model based shape prediction from a combination of direct observations and various surrogates: Application to orthopaedic research. Med. Image Anal. (2012), http://dx.doi.org/10.1016/j.media.2012.04.004

Rao, A., Aljabar, P., Rueckert, D., 2008a. Hierarchical statistical shape analysis and prediction of sub-cortical brain structures. Med. Image Anal. 12 (1), 55–68.

Rao, A., Aljabar, P., Rueckert, D., 2008b. Hierarchical statistical shape analysis and prediction of sub-cortical brain structures. Med. Image Anal. 12 (1), 55–68.

Rao, A., Babalola, K., Rueckert, D., 2006. Canonical correlation analysis of sub-cortical brain structures using non-rigid registration. Biomed. Image Registrat., 66–74.

Rohlfing, T., Sullivan, E.V., Pfefferbaum, A., 2009a. Regression models of atlas appearance. Inform. Process Med. Imag. 21, 151–162.

Rohlfing, T., Sullivan, E.V., Pfefferbaum, A., 2009b. Subject-matched templates for spatial normalization. Med. Image Comput. Comput. Assist. Intervent. 12 (Pt 2), 224–231.

Rubin, P., Leyvraz, P., Aubaniac, J., Argenson, J., Esteve, P., de Roguin, B., 1992. The morphology of the proximal femur. A three-dimensional radiographic analysis. J. Bone Joint Surg. Brit. 74-B (1), 28–32.

Schumann, S., Puls, M., Ecker, T., Schwaegli, T., Stifter, J., Siebenrock, K.-A., Zheng, G., 2010. Determination of pelvic orientation from ultrasound images using patch-SSMS and a hierarchical speed of sound compensation strategy. Inform. Process. Comput. – Assist. Intervent., 157–167.

Schünke, M., Schulte, E., Ross, L.M., Schumacher, U., Lamperti, E.D., Rude, J., Voll, M., Telger, T.C., Wesker, K., 2006. Thieme Atlas of Anatomy: General Anatomy and Musculoskeletal System. Thieme.

Seiler, C., Pennec, X., Ritacco, L., Reyes, M., 2010. Femur specific polyaffine model to regularize the log-domain demons registration. In: 10th SPIE Medical Imaging, 2010.

Seiler, C., Weber, S., Schmidt, W., Fischer, F., Reimers, N., Reyes, M., 2009. Automatic landmark propagation for left and right symmetry assessment of tibia and femur: a computational anatomy based approach. In: Annual Meeting of the International Society for Computer Assisted Surgery.

Sierra, R., Zsemlye, G., Székely, G., Bajka, M., 2006. Generation of variable anatomical models for surgical training simulators. Med. Image Anal. 10 (2), 275–285.

Tajima, G., Nozaki, M., Iriuchishima, T., Ingham, S.J., Shen, W., Smolinski, P., Fu, F.H., 2009. Morphology of the Tibial insertion of the posterior cruciate ligament. J. Bone Joint Surg. Am 91 (4), 859–866.

Task Group on Control of Radiation Dose in Computed Tomography, 2000. Managing patient dose in computed tomography. a report of the international commission on radiological protection. Ann ICRP 30 (4), 7–45.

Vercauteren, T., Pennec, X., Perchant, A., Ayache, N., 2008. Symmetric log-domain diffeomorphic registration: a demons-based approach. In: Medical Image Computing and Computer-Assisted Intervention – MICCAI. pp. 754–761. <http://dx.doi.org/10.1007/978-3-540-85988-8_90>.

Weisberg, S., 2005. Applied linear regression. Math. Soc. Sci. 3 (1).

Yang, Y.M., Rueckert, D., Bull, A.M.J., 2008. Predicting the shapes of bones at a joint: application to the shoulder. Comput. Methods Biomech. Biomed. Eng. 11 (1), 19–30.

Zheng, G., Dong, X., Rajamani, K.T., Zhang, X., Styner, M., Thoranaghatte, R.U., Nolte, L.-P., Ballester, M.A.G., 2007. Accurate and robust reconstruction of a surface model of the proximal femur from sparse-point data and a dense-point distribution model for surgical navigation. IEEE Trans. Biomed. Eng. 54 (12), 2109–2122.

Zheng, G., Gollmer, S., Schumann, S., Dong, X., Feilkas, T., Ballester, M.A.G., 2009. A 2d/3d correspondence building method for reconstruction of a patient-specific 3d bone surface model using point distribution models and calibrated X-ray images. Med. Image Anal. 13 (6), 883–899 (includes Special Section on Computational Biomechanics for Medicine).

Please cite this article in press as: Blanc, R., et al. Statistical model based shape prediction from a combination of direct observations and various surrogates: Application to orthopaedic research. Med. Image Anal. (2012), http://dx.doi.org/10.1016/j.media.2012.04.004